Effect of the lattice dynamics on the electronic structure of paramagnetic NiO within the disordered local moment picture

Elham Mozafari,[1,*] Björn Alling,[1,2] Maxim P. Belov,[3] and Igor A. Abrikosov[1]
[1]*Department of Physics, Chemistry and Biology, Linköping University, SE-58183 Linköping, Sweden*
[2]*Max-Planck-Institut für Eisenforschung GmbH, 40237 Düsseldorf, Germany*
[3]*Materials Modeling and Development Laboratory, NUST "MISIS", 119049 Moscow, Russia*

(Received 7 March 2017; revised manuscript received 12 November 2017; published 24 January 2018)

Using the disordered local moments approach in combination with the *ab initio* molecular dynamics method, we simulate the behavior of a paramagnetic phase of NiO at finite temperatures to investigate the effect of magnetic disorder, thermal expansion, and lattice vibrations on its electronic structure. In addition, we study its lattice dynamics. We verify the reliability of our theoretical scheme via comparison of our results with available experiment and earlier theoretical studies carried out within static approximations. We present the phonon dispersion relations for the paramagnetic rock-salt (B1) phase of NiO and demonstrate that it is dynamically stable. We observe that including the magnetic disorder to simulate the paramagnetic phase has a small yet visible effect on the band gap. The amplitude of the local magnetic moment of Ni ions from our calculations for both antiferromagnetic and paramagnetic phases agree well with other theoretical and experimental values. We demonstrate that the increase of temperature up to 1000 K does not affect the electronic structure strongly. Taking into account the lattice vibrations and thermal expansion at higher temperatures have a major impact on the electronic structure, reducing the band gap from ∼3.5 eV at 600 K to ∼2.5 eV at 2000 K. We conclude that static lattice approximations can be safely employed in simulations of the paramagnetic state of NiO up to relatively high temperatures (∼1000 K), but as we get closer to the melting temperature vibrational effects become quite large and therefore should be included in the calculations.

DOI: 10.1103/PhysRevB.97.035152

I. INTRODUCTION

Transition metal oxides (TMO) exhibit a rich variety of electronic and magnetic properties, ranging from being insulators to metals or even superconductors, from Pauli paramagnetism to local moment behavior of ferromagnetic or antiferromagnetic phases [1]. They range from TiO_2 with a nominal $3d^0$ configuration to Cu_2O with a closed $3d^{10}$ shell, from nonmagnetic insulators (TiO_2) to ferromagnetic half-metallic CrO_2 [2]. In addition, changes of temperature, pressure, or composition, as well as deliberate doping of these materials can modify their electronic and magnetic structure dramatically. It is a challenging task to study these systems by means of a first-principles electronic structure theory as the partially filled, rather localized, *d* shell of the transition metals contain strongly correlated electrons while the *s* and *p* shells of oxygen contain delocalized electrons. In particular, NiO has been the subject of research for over 80 years [3]. It has a large band gap of 4.3 eV with the Néel temperature of $T_N = 523$–530 [4–6] above which NiO is paramagnetic (PM) with a rock-salt (B1) crystal structure. Below this temperature, NiO has antiferromagnetic (AFM) ordering with a small rhombohedral distortion from its cubic structure. It has been considered as a prototype Mott insulator [7,8] after Mott showed that NiO and other similar insulators are better described within the picture of localized electrons bound to partially filled shells. The experimental observation of the Mott insulator-to-metal (IMT) transition in NiO at 240 GPa by resistance measurements has been reported by Gavriliuk *et al.* [9], but the presence of the transition at pressure below 280 GPa has been questioned by Potapkin *et al.* [10], who observed magnetic hyperfine splitting that confirms the antiferromagnetic state of NiO up to 280 GPa, the highest pressure where magnetism has been observed so far, in any material. In fact, recent calculations by Leonov *et al.* predict that in NiO the magnetic collapse should occur at a remarkably higher pressure of ∼429 GPa [11]. Moreover, since Fujimori and Minami could explain NiO photoemission data using a cluster approach with a configuration interaction model, NiO was considered as a charge transfer insulator [12]. Thus, despite all the experimental and theoretical research [1,8,11,13–20] carried out on NiO, investigations of its electronic structure still attract substantial interest. On one hand, using band theories, which are based on the delocalized nature of the electrons, predict NiO to be metallic [21]. On the other hand, due to the strong correlation between the *d* electrons conventional density functional theory (DFT) in the framework of local density approximation (LDA) or generalized gradient approximation (GGA), are not applicable resulting in too small band gaps and local magnetic moment as compared to experimental values. Self-consistent *GW* [22] calculations on NiO do not properly reproduce the experimental spectra [23,24]. The LDA+*U* [25] approach has significantly improved the band structure theory of strongly correlated systems. However, the static LDA+*U* calculations do not take into account the effects of electron dynamics on the electronic structure and might for

*elhmo@ifm.liu.se

this reason not adequately produce the energy spectrum of NiO, especially in its paramagnetic state. A combination of LDA and dynamical mean field theory (DMFT), LDA+DMFT [4,11,26–29], can be used to study the photoemission spectra of NiO which provide a more accurate scheme. Indeed, analysis of orbitally resolved spectra showed [26] that the LDA+DMFT description is superior to the LDA+U. In particular, the LDA+DMFT is able to realistically capture the distribution of spectral weight between different peaks in the photoemission spectra. Moreover, Panda *et al.* [19] used a combination of DMFT and GW to get a better description of the photoemission spectra of NiO. Eder applied the variational cluster approximation to the calculation of the single-particle spectral function of NiO [30]. The LDA+DMFT calculations that includes the Ni d and O p orbitals (the so-called p-d model) give a description of the spectral properties of NiO, which are consistent with cluster calculations [12,30] within their respective limitations.

The studies that focused on the AFM phase attributed the insulating gap to the long-range magnetic order. However, it is now well known that neither the band gap nor the local magnetic moment typically change dramatically when the temperature is raised above the Néel temperature. The LDA+DMFT is generally believed to give the best description of real systems close to the Mott-Hubbard metal-insulator transition (MIT) [31], but if the lattice dynamics is to be included, the calculations would be computationally extremely demanding. An alternative approach could be to use the LDA+U which is computationally less demanding than LDA+DMFT. Although LDA+U is considered as a reliable method within which the magnetically ordered phases can be simulated easily, it is believed not to be suitable for the simulations of the magnetically disordered PM state. However, its combination with the disordered local moment (DLM) picture opens up a possibility for such a study. This is the approach we use in the present work. We are therefore led to a question on the possibility of simulating the PM insulating phase of NiO, which should also include other types of excitations and in particular lattice vibrations.

The disordered local moments molecular dynamics (DLM-MD) method is an implementation of the DLM picture within the framework of *ab initio* molecular dynamics (MD). The idea was developed by Steneteg *et al.* [32]. DLM-MD is shown to be a reliable method to simulate magnetic materials in their paramagnetic state [32–34]. In this work we investigate the electronic structure of PM NiO using DLM-MD in which the magnetic disorder and the lattice vibrations are treated simultaneously. In order to verify our theoretical tools, we compare the obtained energy spectra with the ones obtained from other theoretical schemes and also with the experimental photoemission spectra (available only for a magnetically ordered phase). We study the explicit effects of lattice vibrations on the electronic density of states of NiO and we derive the vibrational phonon spectra of PM NiO at elevated temperatures.

II. COMPUTATIONAL DETAILS

The theoretical background of the DLM picture and its implementation in the magnetic sampling method, as well as in the DLM-molecular dynamics, have been discussed in detail in Ref. [32]. Thus, here we mainly focus on the technical details of the calculations and on the method's limitations. Starting from the DLM idea of having spatially disordered local moments, we prepare a supercell in which the local magnetic moments on metal atoms (Ni in our study) are randomly oriented in up and down directions. $T = 0$ K calculations are done using DLM in combination with a magnetic sampling method (DLM-MSM) [35]. In this method a series of static DLM calculations are run, each with a random magnetic configuration which is different from other magnetic configurations in the series. The density of states is then obtained by averaging DOSs from these calculations.

For DLM-MD calculations, we fix the magnetic subsystem at a specific magnetic configuration for an interval time which we call spin flip time $t_{\rm sf}$. We then run MD calculations for $t_{\rm MD}$ time steps. The number of the MD steps during which the magnetic configuration is kept fixed can be obtained by $N^{\rm sf}_{\rm MD} = t_{\rm sf}/t_{\rm MD}$. After $N^{\rm sf}_{\rm MD}$ time steps, the orientation of the magnetic moments is changed to another random configuration and the calculations continue with this new magnetic configuration for the next $N^{\rm sf}_{\rm MD}$ time steps. In our simulations we have chosen $t_{\rm sf} = 5$ fs and $t_{\rm MD} = 1$ fs and run the calculations for the total number of 5000 steps (5 ps). This corresponds to a rapid change of the magnetic state on the time scale of the vibrational periods meaning that the trajectories of the atoms are effectively determined by forces averaged over magnetic degrees of freedom, making the approach close to the adiabatic limit of a very fast magnetic degree of freedom. We have carried out the DLM-MD calculations at 600, 1000, and 2000 K and the local spin density approximation is used together with the Hubbard Coulomb term (LDA+U) following the Dudarev scheme [36]. We have tested the LDA+U method with different $U^{\rm eff}$ values and compared the obtained electronic structure with that of the experiment and the electronic spectrum from LDA+DMFT calculations. Based on this comparison, we have chosen the value $U^{\rm eff} = 8$ eV ($U^{\rm eff} = U - J$) with $U = 9$ and $J = 1$ eV.

Beside using the DLM-LDA+U approach to describe the paramagnetic state, it is worth to point out the additional important underlying assumptions of the DLM-MD method. In particular, the local magnetic moments are considered to be collinear and therefore the effect from the noncollinearity of the moments is neglected. This assumption is well justified for the simulations of the paramagnetic state with disordered local moments as long as the temperature of the simulation is much larger than the strongest interaction of the classical Heisenberg Hamiltonian ($T \gg J^{\rm max}_{ij}$) [37]. Therefore, we assume that the local magnetic moments exist above the magnetic transition temperature, and they are fully disordered and collinear. In addition, we note that in the DLM-MD, the true spin dynamics is substituted by instantaneous alteration of the sample magnetic configuration with time steps $t_{\rm sf}$. In other words, within the DLM model [37], it is assumed that for a duration of $t_{\rm sf}$ the system gets stuck near points (in the phase space) with finite moments at every magnetic site (Ni ions in our case) oriented in more or less random directions and then rapidly moves to another similar point. This means that the ergodicity is temporarily broken. However, according to Ref. [37], the system is in fact ergodic even though it does not cover the phase space uniformly in time and the motion of the temporarily broken ergodicity can be mainly attributed to the changes in the orientational configuration of the local

moments. One very important factor to point out is that the goal of supercell calculations is to approximate the self-averaging extensive physical properties of a paramagnetic alloy at finite temperatures, like the potential energy, the magnetic moments, or the electronic density of states. Indeed, if the criteria for the applicability of the DLM is fulfilled, i.e., $T \gg J_{ij}^{\max}$, the self-averaging extensive physical properties can be calculated from the arithmetic average of different magnetic configurations. In other words, DLM-MD is about obtaining the right averages rather than right trajectories in the phase space. A very detailed description of the DLM-MD method can be found in Ref. [38].

In order to obtain the density of states, we have chosen a series of 25 uncorrelated samples from our DLM-MD and calculated the DOS for each of them separately. The resulting electronic structure is the average DOS of these calculations. A similar averaging procedure has been adopted in the DLM-MSM calculations. Note that we do not include the Fermi smearing effects in the DOS plots to focus the discussion on the effects of lattice vibrations.

The AFM phase is simulated using a four-atom rhombohedral unit cell with AFM ordering consisting of alternating (111) planes with collinear spin up and spin down orientations. A Monkhorst-Pack $23 \times 23 \times 23$ k-point grid is used to sample the Brillouin zone and the energy cutoff is set to 500 eV.

For the PM phase, we have used a $2 \times 2 \times 2$ conventional cubic supercell containing 32 Ni atoms with collinear up and down spins randomly oriented on Ni atoms, and 32 O atoms. The Brillouin zone is sampled using a Monkhorst-Pack $3 \times 3 \times 3$ k-point grid and the energy cutoff is set to 500 eV.

To maintain the temperature during our DLM-MD simulations we have used a canonical ensemble (NVT) and the Nosé thermostat with the default mass as implemented in the Vienna *ab initio* simulation package (VASP) [39]. Thermal expansion is included in our calculations using the experimental lattice spacings [40].

To extract the vibrational frequencies of the high temperature PM NiO phase from the molecular dynamics simulations we have used the temperature dependent effective potential (TDEP) method recently developed by Hellman *et al.* [41,42] and combined it with the DLM-MD method by Shulumba *et al.* [34]. In the framework of this method we have calculated the temperature dependent dynamical matrices by least square fitting of the forces of the harmonic Hamiltonian [41,42] to forces from DLM-MD, calculated at the proper atomic displacements. The procedure included the information collected at each of the 5000 MD time steps. It was carried out at 500 and 1000 K. Moreover, we have corrected the long range interaction of the macroscopic electric field induced by polarization of collective ionic motions near the Γ point, adding a nonanalytical term [43–45] to the dynamical matrix and in this way obtaining the LO-TO splitting. In order to obtain the complete dynamical matrix at $q = 0$ including the nonanalytical terms, we determined the Born effective charges $[Z^*(\mathrm{Ni}), Z^*(\mathrm{O})]$ and dielectric (ε^{∞}) tensors by means of the density functional perturbation theory as implemented in VASP. For averaging values of $[Z^*(\mathrm{Ni}), Z^*(\mathrm{O})]$ and (ε^{∞}), six zero temperature calculations have been made for the ideal NaCl-type supercell crystal structures, each with a random magnetic configuration, that has allowed us to obtain the tensors in the right form corresponding to the cubic symmetry.

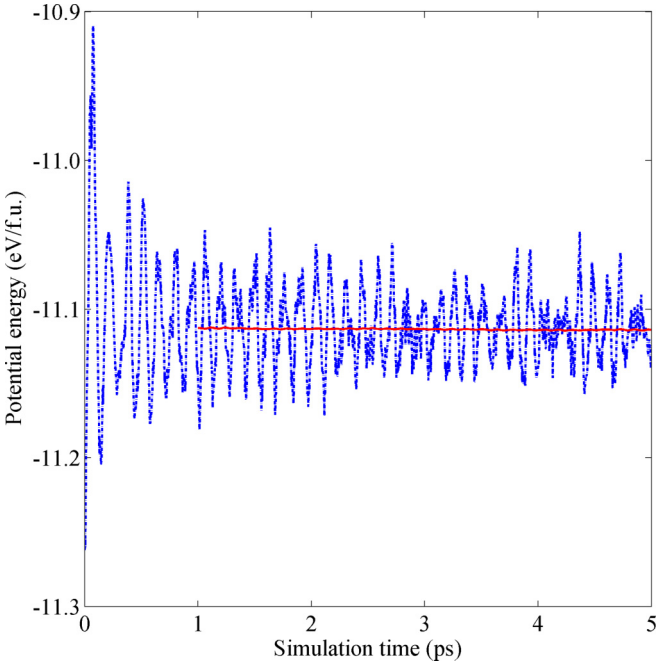

FIG. 1. Time evolution of the potential energy of the cubic paramagnetic NiO at $T = 600$ K (blue dashed line) extracted from the DLM-MD calculation. The accumulated average of the potential energy is shown with a red solid line. The equilibration time of 1 ps is not included in calculations of the running average. The potential energy is stable and well converged as is seen from the running average.

III. RESULTS

A. The potential energy

One way to check the reliability of the calculations is to check if the energy of the system from the DLM-MD is stable and that its mean value converges. Figure 1 shows the behavior of the potential energy from the DLM-MD calculation of the PM NiO at $T = 600$ K (blue dashed line) for all the MD steps. The energy shows rather large variation in the beginning but after about 1 ps the fluctuations in the potential energy become quite small. The accumulated average (red solid line) of the potential energy after equilibration ($\sim$1 ps) is also shown and it is apparent the potential energy of the system is stable and the mean value is well converged. Similar behavior is observed for other temperatures (not shown here).

B. Magnetic moments

During DLM-MD calculations, the magnitude of the local magnetic moments are allowed to vary in accordance with the self-consistent solution of the electronic structure problem at each step of the MD simulation. Strictly speaking, the magnetic moments are allowed to flip and there is no restriction on their orientations. However, in this work they can only align in up and down directions (collinear spin configurations). In any case, it is important to check the net magnetization of the system to make sure it remains near zero, indicating

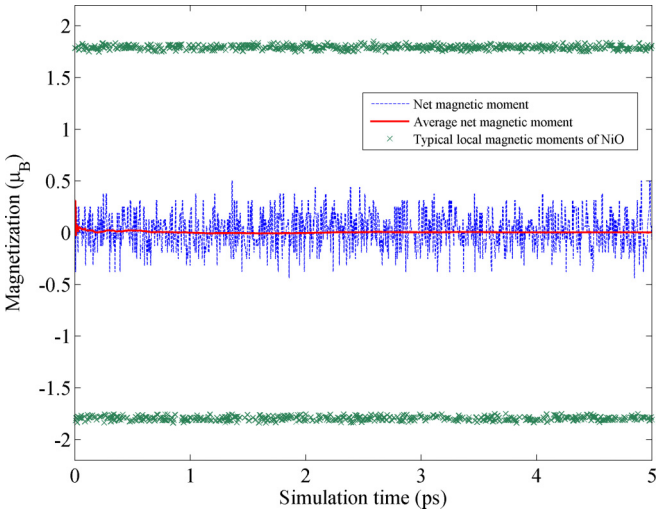

FIG. 2. Time evolution of the net magnetic moment per supercell (blue dashed line), its accumulated average (red solid line), and the local magnetic moment of a single Ni atom (green dots) for the cubic paramagnetic NiO at $T = 600$ K from the DLM-MD calculation.

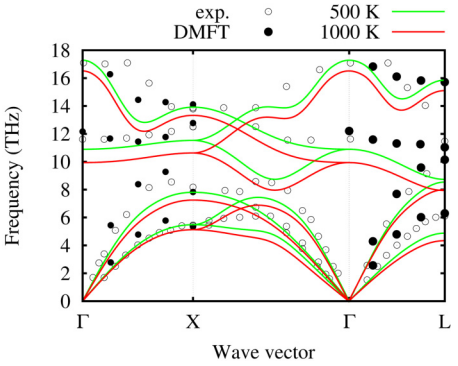

FIG. 3. Phonon spectra of PM NiO at 500 K (green lines) and 1000 K (red lines), filled circles represents DMFT results [50]. Experimental data for AFM phase measured at 297 K [51] presented as open circles.

that the simulated system remains in the DLM state during the whole simulation. Figure 2 shows the time evolution of the net magnetic moment per supercell (blue dashed line) in μ_B extracted from DLM-MD calculations of the PM NiO at $T = 600$ K. The accumulated average of the net magnetization (red solid line) is also shown. For further information, we also demonstrate the variation of the local magnetic moment of a single Ni atom as a function of simulation time (green dots). As mentioned earlier, the spins are aligned in up and down directions having equal positive and negative values. This is shown in Fig. 2 by two series of green dots with the average absolute value of 1.759 μ_B. We observe a similar behavior in the magnetization via DLM-MD calculations at other temperatures (not shown here).

From our calculations, the average local magnetic moment of Ni ions in the AFM phase is 1.764 μ_B. These values are in very good agreement with other experimental [46] and theoretical studies [4,47] for both phases, and correspond to the high-spin magnetic state of the Ni^{2+} ($3d^8$) ions in a cubic crystal field. We can therefore conclude that neither the magnetic disorder and the AFM-PM phase transition nor explicit lattice vibrations have a prominent impact on the value of the local magnetic moment, in line with our previous studies on the localized magnetic moments on Cr atoms in a CrN ceramic system [48] but in contrast to the case of more itinerant elemental pure Fe [49].

C. Phonon dispersion relations

We have calculated the phonon dispersion relations of the PM NiO at two different temperatures, just below its magnetic ordering temperature at 500 K and well above it at 1000 K. For the LO-TO splitting we used the following calculated static dielectric properties: $Z^*_{xx}(\mathrm{Ni}) = Z^*_{yy}(\mathrm{Ni}) = Z^*_{zz}(\mathrm{Ni}) = 2.158 \pm 0.006e$, $Z^*_{xx}(\mathrm{O}) = Z^*_{yy}(\mathrm{O}) = Z^*_{zz}(\mathrm{O}) = -2.151 \pm 0.008e$, $\varepsilon^\infty_{xx} = \varepsilon^\infty_{yy} = \varepsilon^\infty_{zz} = 5.002 \pm 0.009$, all off-diagonal tensors components are almost equal to zero, as it must be in a cubic crystal. The results for both temperatures are shown in Fig. 3.

We see that the PM phase is dynamically stable in the whole investigated temperature range, giving additional justification to the reliability of our computational approach. Interestingly, the PM phase of NiO is dynamically stable even at a temperature where the AFM phase is found experimentally. This means that there are no dynamical instabilities or phonon softening in the PM phase of NiO that are directly responsible for a simultaneous magnetic and structural transition observed in NiO at the Néel temperature. In fact, a strong softening is observed in our calculations with increasing temperature, especially in the optical part of the spectrum.

Unfortunately, we are not aware of any high-quality experimental measurements of the phonon dispersion relations in the PM NiO. However, the phonon spectra of the AFM NiO phase were measured by Coy *et al.* [51] at 297 K. They observed a well-defined band gap of approximately 1.6 THz. In addition, Coy *et al.* mentioned the preliminary measurements above the Néel temperature at 600 K. The authors of Ref. [51] indicated that they did not expect large effects of the magnetic transition on the phonon spectrum of NiO, besides a general temperature-induced softening with lattice frequencies reduced typically by about 3%. This conclusion is generally supported by good agreement that can be seen for acoustic branches of the phonon spectrum between our calculations for the PM NiO and Coy *et al.* [51] measurements for the AFM samples. On the other hand, our paramagnetic optical dispersion relations differ from the experimental AFM ones to a larger degree.

Our calculated value of $\varepsilon^\infty = 5.002$ is close to the experimental value of 5.7 for the AFM phase [52]. The low-frequency dielectric constant ε^0 can be calculated from the Lyddane-Sachs-Teller relation [53] for the cubic system: $\omega^2_{\mathrm{LO}}/\omega^2_{\mathrm{TO}} = \varepsilon^0/\varepsilon^\infty$. The calculated value at $T = 500$ K ($\varepsilon_0 = 12.6$) is close to the experimental $\varepsilon^0 = 11.75$ value for the AFM phase [52].

Phonon spectra of the PM phase of NiO was calculated in the framework of DMFT in Ref. [50]. As expected, the latter reproduce the experimental results more accurately, because of a more accurate description of the electronic structure of NiO within the DMFT in comparison with LDA+U calculations, which we discuss below in more detail. Still, our DLM-MD-LDA+U results satisfactory reproduce DMFT

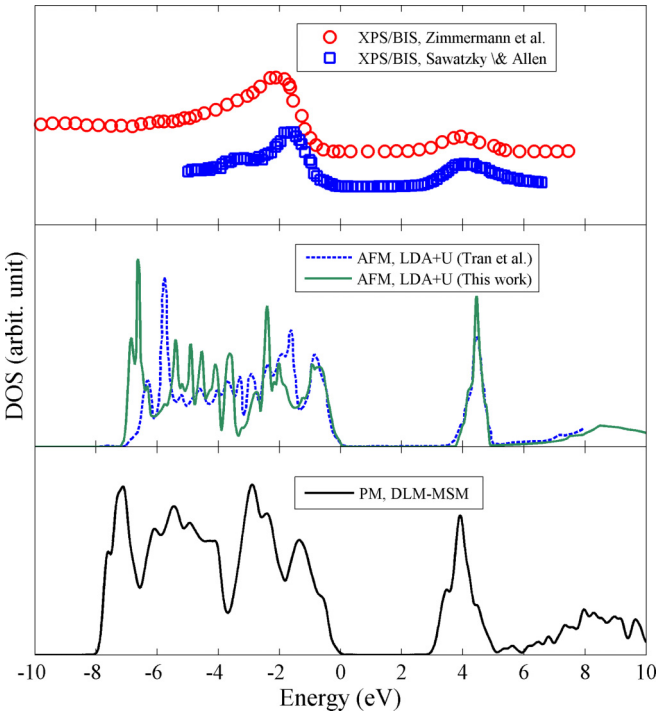

FIG. 4. Electronic structure of antiferromagnetic NiO from experiment (top panel, red circles from Ref. [1] and blue dots from Ref. [13]) and theory (middle panel, green solid line denotes results of this work, blue dashed line is from Ref. [20]) as well as for paramagnetic NiO extracted from DLM-MSM calculations (bottom panel). The theoretical calculations in this work are carried out at $T = 0$ K using the LDA+U method with $U^{\text{eff}} = 8$ eV (note that calculations in Ref. [20] were carried out with $U^{\text{eff}} = 7$ eV). The lattice constant used in the calculations is the same as the 0 K experimental value $a = 4.17$ Å. The zero energy point corresponds to the top of the valence band.

phonon dispersion relations. In comparison with the experiment, our calculations underestimate the experimental frequencies while the DMFT in general overestimates them, though to a smaller degree. Partly this disagreement can be explained by the softening of the lattice with temperature, which is revealed in our calculations. Indeed, DMFT results were obtained at zero ionic temperature, experimental data were taken at 297 K (in magnetically ordered state), while our calculations were carried out at 500 and 1000 K. In fact, it would be desirable to carry out more accurate measurements of the phonon dispersion relations in the paramagnetic phase of NiO.

D. The electronic structure

We have calculated the electronic structure of both AFM and PM phases of NiO. The results at 0 K for both phases are shown in Fig. 4. The experimental XPS-BIS data for the AFM phase at room temperature is also shown for comparison. One can see that our results for both AFM and PM phases are in reasonable agreement with the experimental data. The band gap of the AFM and PM phases from our calculations are about 4.6 and 4.3 eV, respectively, in qualitative agreement with the experimental value of 4.3 eV [13]. The valence bandwidth of ∼8 eV is in agreement with other theoretical [18,20,54] studies. Our calculated results for AFM NiO demonstrate that the LDA+U approach with the chosen set of parameters can be used to study the electronic structure of paramagnetic NiO using our DLM-based methods.

Let us start with static calculations using the DLM-MSM method which mimics as close as possible state-of-the art calculations for the ordered AFM phase, as well as calculations carried out using the DFT+DMFT. Indeed, the DLM-MSM calculations are performed nominally for static though magnetically disordered supercells. In this respect, the DLM-MSM calculations purify the effect of magnetic disorder.

It is generally believed that the magnetic disorder does not affect the electronic structure of NiO [55,56] and the electronic structure of the PM NiO is often compared to that of the experimental low-temperature AFM phase. In general, our calculations support this conclusion. However, considering the results shown in Fig. 4 in detail one can see that the band gap is affected by the magnetic phase transition in NiO and becomes smaller in the PM phase. Even though the difference between the AFM and PM electronic structures is not huge and the band gaps differ by only about 0.3 eV, for quantitative calculations, it is important to consider the specific magnetic state of relevance for the particular temperature of interest. Within our DLM-MSM calculations, this effect is taken into account and we can therefore successfully distinguish this small difference. A very interesting point to note here is that our DLM-MSM method shows certain effects of the magnetic disorder when the lattice temperature is $T = 0$ K.

An additional check for the validity of our calculations can be done by comparing our obtained electronic structure using the DLM-MSM method with the results obtained from other theoretical methods such as LDA+DMFT. This comparison is of interest because the effect of magnetic disorder is included in both approaches. However, within DMFT, the magnetic disorder is treated in a formally correct though single site and mean-field way while in the DLM-MSM it is included within the concept of the temporarily broken ergodicity including magnetically different local environments. Figure 5 (top panel) displays the results from such a comparison. It is seen that the LDA+DMFT method gives a more accurate description of the electronic structure of NiO in terms of, e.g., valence band width and the spectral weight between different peaks in the spectra. In fact, there is a qualitative difference in the orbital resolved spectra obtained by the two approaches. In Fig. 5 (bottom panel) we show DOS of NiO projected onto t_{2g}, and e_g orbitals of Ni, as well as on p orbitals of O. Note that the results of our static LDA+U calculations agree well with recent static DLM calculations by Trimarchi *et al.* [57]. While DMFT exhibits a Ni-d peak at low binding energy [11], LDA+U with $U_{\text{eff}} = 8$ eV places the Ni d-band weight at high binding energy. This effect is more pronounced for the t_{2g} orbitals with weaker p-d hybridization. Still, the main features of the DOS essential for this study, including the presence of the band gap in the paramagnetic state, are well reproduced in our LDA+U calculations combined with the DLM-MSM description of magnetic disorder. We note that the plane LDA+U method is believed to be unsuitable for the description of the paramagnetic state. We therefore conclude that although not as accurate as LDA+DMFT calculations, the approach proposed here is robust and gives a qualitatively good

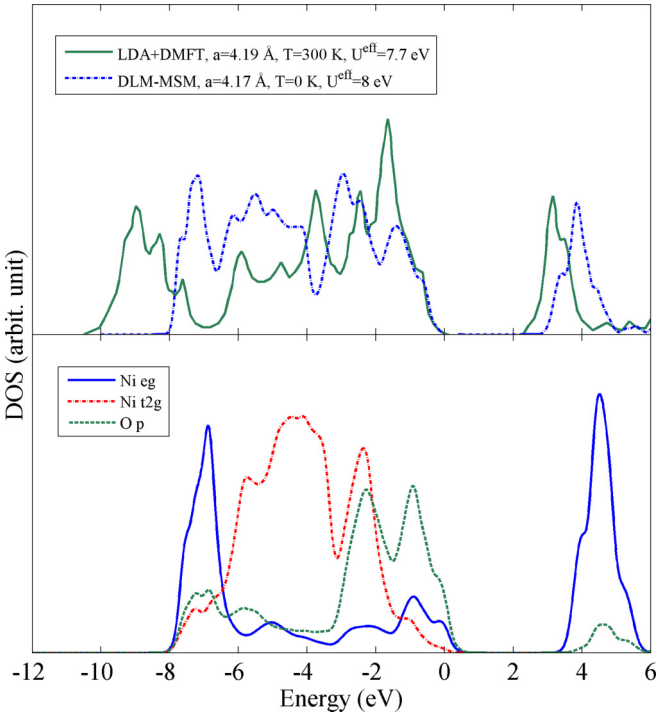

FIG. 5. Top panel: Comparison of the density of states (DOS) of paramagnetic NiO from DLM-MSM calculations (blue dot-dashed line) with the DOS from the LDA+DMFT calculations from Ref. [19] (red solid line). Bottom panel: DOS of NiO calculated with the DLM-MSM method ($U_{\text{eff}} = 8$ eV) projected onto t_{2g} and e_g orbitals of Ni, as well as on p orbitals of O. The zero energy point corresponds to the top of the valence band.

picture of the electronic density of states for such a prototypical strongly correlated paramagnetic solid as NiO.

Let us next proceed towards a more detailed study of the effects of the lattice vibrations coupled to the magnetic disorder at higher temperatures. The DLM-MD method combined with the LDA+U technique provides us with the opportunity to study these effects simultaneously. We have used DLM-MD at different temperatures to check the impact of the lattice vibrations and the temperature on the electronic structure of the PM phase of NiO.

Figure 6 compares the results from the static DLM-MSM calculations at $T = 0$ K and the electronic structure from the DLM-MD calculations at $T = 600$ K taking, in addition to the atomic vibrations of the MD, the thermal expansion effect into account through the experimental temperature dependence of the lattice constant. As it is observed and expected, a relatively small temperature increase, up to 600 K, does not have a large influence on the electronic structure of NiO. However, at higher temperatures (Fig. 7) the effect of lattice vibrations becomes more prominent. Indeed, the band gap becomes visibly smaller at $T = 2000$ K, just below the NiO melting temperature of 2230 K [58]. One would wonder whether this apparent change comes from the lattice vibrations or is it due to the thermal expansion of the crystal lattice. To answer this question, we run a DLM-MSM calculation with atoms on static lattice positions but with the lattice constant from $T = 2000$ K, i.e., $a = 4.28$ Å and compared it with our

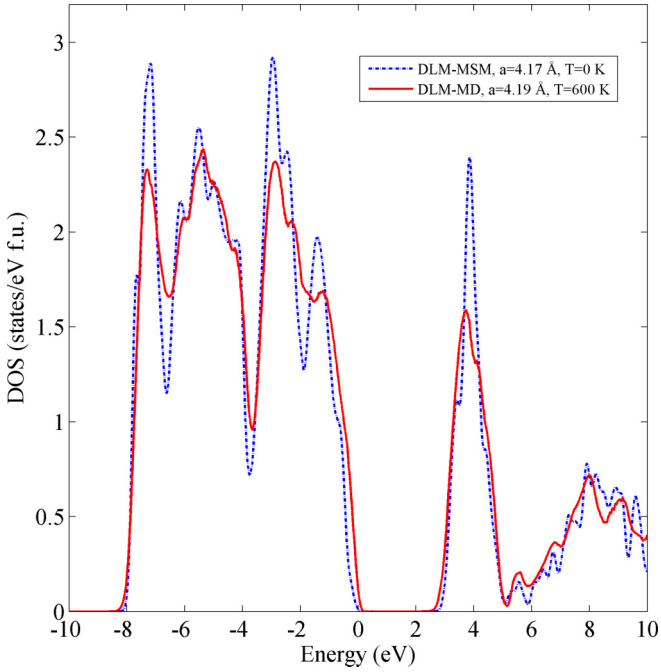

FIG. 6. Comparison of the density of states (DOS) of paramagnetic NiO at $T = 600$ K obtained from the DLM-MD calculation with the static DLM-MSM calculations at $T = 0$ K. The thermal expansion is included via experimental lattice spacing at different temperatures. The zero energy point is set to the top of the valence band.

DLM-MSM result obtained for the zero temperature lattice constant $a = 4.17$ Å. The comparison is shown in Fig. 8. What is seen from the obtained density of states plots in Fig. 8 suggests that the impact from the thermal expansion is not

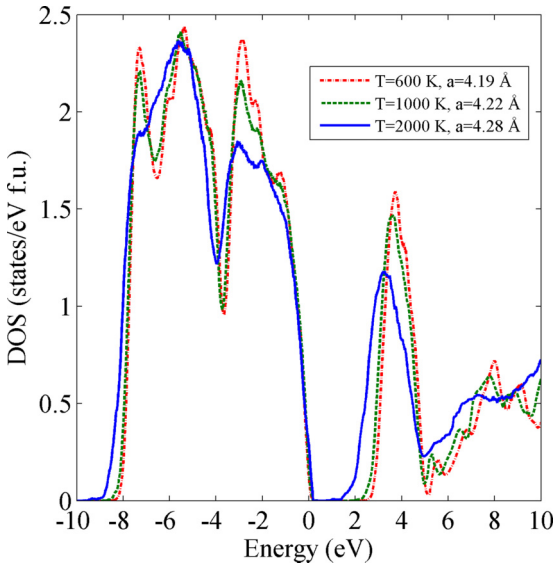

FIG. 7. Comparison of the density of states (DOS) of paramagnetic NiO obtained from the DLM-MD at three different temperatures: $T = 600$ K (red dot-dashed line), $T = 1000$ K (green dashed line), and $T = 2000$ K (blue solid line). The thermal expansion is included via experimental lattice spacing at different temperatures. The zero energy point is set to the top of the valence band.

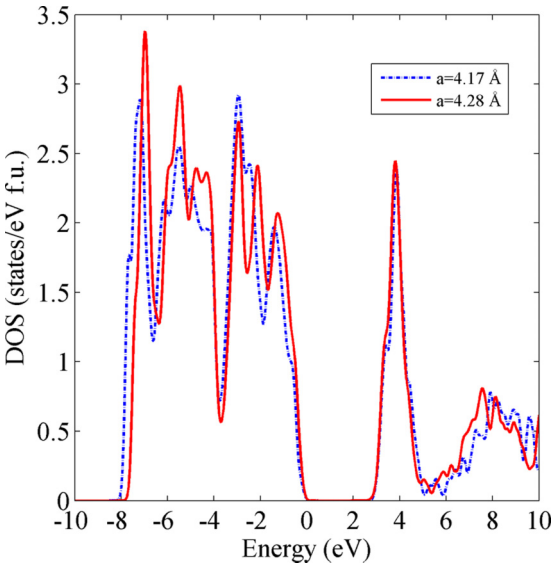

FIG. 8. Comparison of the density of states (DOS) of paramagnetic NiO obtained from the DLM-MSM calculations at $T = 0$ K using two different lattice spacings, 0 K lattice parameter $a = 4.17$ Å (blue dashed-dot line) and 2000 K lattice parameter $a = 4.28$ Å (red solid line). The zero energy point is set to the top of the valence band.

large and therefore we conclude that the change in the spectrum obtained at temperatures around the melting temperature from the DLM-MD simulations should be attributed explicitly to lattice vibrations. In other words, including lattice vibrations at higher temperatures along with the magnetic excitations has a prominent impact on the electronic structure of the PM phase of NiO and hence cannot be ignored in predictions of its high-temperature properties.

IV. CONCLUSION

We have combined the LDA+U approach with two recently developed methods based on the disordered local moment picture, the DLM in combination with the magnetic sampling method with atoms sitting at a static lattice, and the DLM-MD with atoms moving at finite temperature to simultaneously treat the magnetic disorder and lattice vibrations in the paramagnetic phase of NiO.

We have calculated the electronic structure of both antiferromagnetic and paramagnetic phases of NiO. We observed that the electronic structure of the PM phase neglecting lattice vibrations, does not differ too much from that of the AFM phase. However, certain effects of the magnetic disorder can be observed even without an explicit consideration of lattice vibrations and they should be taken into account for a more exact and detailed study. In particular, we observe that the magnetic disorder can have a visible effect on the band gap.

To obtain the electronic structure at finite temperatures, we used the DLM-MD method. As expected, we see that changes in the temperature up to 1000 K does not affect the spectrum with more than a smear out effect but at a higher temperature of 2000 K, still well below the melting temperature of ∼2230 K, the magnetic and lattice excitations have a strong impact. The band gap becomes smaller and the fine structure of the peaks in the density of the state disappears. This change is mostly associated with the explicit effect of lattice vibrations and to a lesser degree with the effect of the thermal expansion. We conclude that in order to obtain the electronic structure of PM NiO at lower and intermediate temperatures, it is safe to use static lattice calculations with the thermal expansion coefficient of the crystal lattice taken into account. As the temperature increases and gets closer to the melting point of NiO, the change in the density of states due to explicit lattice vibrations becomes more apparent and therefore cannot be ignored in the calculations.

ACKNOWLEDGMENTS

The authors would like to acknowledge the financial support from the Swedish Research Council (VR) through Grant No. 2015-04391. Development of theoretical methodology was supported by the Ministry of Education and Science of the Russian Federation Grant No. 14.Y26.31.0005. Simulations of the phonon dispersion relations were supported by the Ministry of Education and Science of the Russian Federation in the framework of Increase Competitiveness Program of NUST "MISIS" (No. K2-2017-080) implemented by a governmental decree dated 16 March 2013, No. 211. B.A. is grateful for the financial support by the Swedish Research Council (VR) through the young researcher grant No. 621-2011-4417 and the international career Grant No. 330-2014-6336 and Marie Sklodowska Curie Actions, Cofund, Project INCA 600398, as well as the Swedish Foundation for Strategic Research (SSF) through the future research leaders 6 program. Moreover, we are thankful for the support from the Swedish Government Strategic Research Area in Materials Science on Functional Materials at Linköping University (Faculty Grant SFOMatLiU No. 2009 00971). We would like to thank the Swedish National Infrastructure for Computing (SNIC) at the National Supercomputer Center (NSC) for providing the computational resources.

[1] R. Zimmermann, P. Steiner, R. Claessen, F. Reinert, S. Hüfner, P. Blaha, and P. Dufek, J. Phys.: Condens. Matter **11**, 1657 (1999).
[2] K. Schwarz, J. Phys. F: Met. Phys. **16**, L211 (1986).
[3] S. S. Bhatnagar and G. S. Bal, J. Indian Chem. Soc. **11**, 603 (1934).
[4] X. Ren, I. Leonov, G. Keller, M. Kollar, I. Nekrasov, and D. Vollhardt, Phys. Rev. B **74**, 195114 (2006).
[5] A. Ayuela, D. J. Klein, and N. H. March, Croat. Chem. Acta **86**, 463 (2013).
[6] T. Chatterji, G. J. McIntyre, and P. A. Lindgard, Phys. Rev. B **79**, 172403 (2009).
[7] N. F. Mott, Proc. Phys. Soc. London Sect. A **62**, 416 (1949).
[8] B. Brandow, Adv. Phys. **26**, 651 (1977).
[9] A. G. Gavriliuk, I. A. Trojan, and V. V. Struzhkin, Phys. Rev. Lett. **109**, 086402 (2012).

[10] V. Potapkin, L. Dubrovinsky, I. Sergueev, M. Ekholm, I. Kantor, D. Bessas, E. Bykova, V. Prakapenka, R. P. Hermann, R. Rüffer, V. Cerantola, H. J. M. Jönsson, W. Olovsson, S. Mankovsky, H. Ebert, and I. A. Abrikosov, Phys. Rev. B **93**, 201110 (2016).
[11] I. Leonov, L. Pourovskii, A. Georges, and I. A. Abrikosov, Phys. Rev. B **94**, 155135 (2016).
[12] A. Fujimori and F. Minami, Phys. Rev. B **30**, 957 (1984).
[13] G. A. Sawatzky and J. W. Allen, Phys. Rev. Lett. **53**, 2339 (1984).
[14] K. Terakura, A. R. Williams, T. Oguchi, and J. Kubler, Phys. Rev. Lett. **52**, 1830 (1984).
[15] K. Terakura, T. Oguchi, A. R. Williams, and J. Kubler, Phys. Rev. B **30**, 4734 (1984).
[16] S. Hufner, P. Steiner, I. Sander, F. Reinert, and H. Schmitt, Z. Phys. B: Condens. Matter **86**, 207 (1992).
[17] E. Z. Kurmaev, R. G. Wilks, A. Moewes, L. D. Finkelstein, S. N. Shamin, and J. Kuneš, Phys. Rev. B **77**, 165127 (2008).
[18] R. Gillen and J. Robertson, J. Phys.: Condens. Matter **25**, 165502 (2013).
[19] S. K. Panda, B. Pal, S. Mandal, M. Gorgoi, S. Das, I. Sarkar, W. Drube, W. Sun, I. Di Marco, A. Lindblad, P. Thunström, A. Delin, O. Karis, Y. O. Kvashnin, M. van Schilfgaarde, O. Eriksson, and D. D. Sarma, Phys. Rev. B **93**, 235138 (2016).
[20] F. Tran, P. Blaha, K. Schwarz, and P. Novák, Phys. Rev. B **74**, 155108 (2006).
[21] L. F. Mattheiss, Phys. Rev. B **5**, 290 (1972).
[22] H. Lars, Phys. Rev. **139**, A796 (1965).
[23] F. Aryasetiawan and O. Gunnarsson, Phys. Rev. Lett. **74**, 3221 (1995).
[24] S. V. Faleev, M. van Schilfgaarde, and T. Kotani, Phys. Rev. Lett. **93**, 126406 (2004).
[25] V. I. Anisimov, F. Aryasetiawan, and I. Lichtenstein, J. Phys.: Condens. Matter **9**, 767 (1997).
[26] J. Kuneš, V. I. Anisimov, A. V. Lukoyanov, and D. Vollhardt, Phys. Rev. B **75**, 165115 (2007).
[27] Q. Yin, A. Gordienko, X. Wan, and S. Y. Savrasov, Phys. Rev. Lett. **100**, 066406 (2008).
[28] M. Karolak, G. Ulm, T. Wehling, V. Mazurenko, A. Poteryaev, and A. Lichtenstein, J. Electron Spectrosc. Relat. Phenom. **181**, 11 (2010).
[29] P. Thunström, I. Di Marco, and O. Eriksson, Phys. Rev. Lett. **109**, 186401 (2012).
[30] R. Eder, Phys. Rev. B **76**, 241103(R) (2007).
[31] K. Held, G. Keller, V. Eyert, D. Vollhardt, and V. I. Anisimov, Phys. Rev. Lett. **86**, 5345 (2001).
[32] P. Steneteg, B. Alling, and I. A. Abrikosov, Phys. Rev. B **85**, 144404 (2012).
[33] B. Alling, L. Hultberg, L. Hultman, and I. A. Abrikosov, Appl. Phys. Lett. **102**, 031910 (2013).
[34] N. Shulumba, B. Alling, O. Hellman, E. Mozafari, P. Steneteg, M. Odén, and I. A. Abrikosov, Phys. Rev. B **89**, 174108 (2014).
[35] B. Alling, T. Marten, and I. A. Abrikosov, Phys. Rev. B **82**, 184430 (2010).
[36] S. L. Dudarev, G. A. Botton, S. Y. Savrasov, C. J. Humphreys, and A. P. Sutton, Phys. Rev. B **57**, 1505 (1998).
[37] B. L. Gyorffy, A. J. Pindor, J. Staunton, G. M. Stocks, and H. Winter, J. Phys. F **15**, 1337 (1985).
[38] E. Mozafari, N. Shulumba, P. Steneteg, B. Alling, and I. A. Abrikosov, Phys. Rev. B **94**, 054111 (2016).
[39] G. Kresse and D. Joubert, Phys. Rev. B **59**, 1758 (1999).
[40] E. Gillam and J. P. Holden, J. Am. Ceram. Soc. **46**, 601 (1963).
[41] O. Hellman, I. A. Abrikosov, and S. I. Simak, Phys. Rev. B **84**, 180301 (2011).
[42] O. Hellman, P. Steneteg, I. A. Abrikosov, and S. I. Simak, Phys. Rev. B **87**, 104111 (2013).
[43] R. Pick, M. Cohen, and R. Martin, Phys. Rev. B **1**, 910 (1970).
[44] P. Giannozzi, S. de Gironcoli, P. Pavone, and S. Baroni, Phys. Rev. B **43**, 7231 (1991).
[45] X. Gonze and C. Lee, Phys. Rev. B **55**, 10355 (1997).
[46] B. E. F. Fender, A. J. Jacobson, and F. A. Wedgwood, J. Chem. Phys. **48**, 990 (1968).
[47] V. I. Anisimov, I. V. Solovyev, M. A. Korotin, M. T. Czyżyk, and G. A. Sawatzky, Phys. Rev. B **48**, 16929 (1993).
[48] E. Mozafari, B. Alling, P. Steneteg, and I. A. Abrikosov, Phys. Rev. B **91**, 094101 (2015).
[49] B. Alling, F. Körmann, B. Grabowski, A. Glensk, I. A. Abrikosov, and J. Neugebauer, Phys. Rev. B **93**, 224411 (2016).
[50] S. Y. Savrasov and G. Kotliar, Phys. Rev. Lett. **90**, 056401 (2003).
[51] R. Coy, C. Tompson, and E. Gürmen, Solid State Commun. **18**, 845 (1976).
[52] P. J. Gielisse, J. N. Plendl, L. C. Mansur, R. Marshall, S. S. Mitra, R. Mykolajewycz, and A. Smakula, J. Appl. Phys. **36**, 2446 (1965).
[53] R. H. Lyddane, R. G. Sachs, and E. Teller, Phys. Rev. **59**, 673 (1941).
[54] H. Jiang, R. I. Gomez-Abal, P. Rinke, and M. Scheffler, Phys. Rev. B **82**, 045108 (2010).
[55] O. Tjernberg, S. Söderholm, G. Chiaia, R. Girard, U. O. Karlsson, H. Nylén, and I. Lindau, Phys. Rev. B **54**, 10245 (1996).
[56] W. Jauch and M. Reehuis, Phys. Rev. B **70**, 195121 (2004).
[57] G. Trimarchi, Z. Wang, and A. Zunger, Phys. Rev. B **97**, 035107 (2018).
[58] J. Neumann, T. Zhong, and Y. Chang, *Binary Alloy Phase Diagrams*, 2nd ed., edited by T. B. Massalski (Materials Information Society, Materials Park, OH, 1990), Vol. 2.